JOURNAL OF MATERIALS SCIENCE 28 (1993) 1503–1508

In situ X-ray diffraction of the early stages of the crystallization of $Fe_{80}B_{20}$

C. BRIZARD, B. RODRICKS, E. ALP
Advanced Photon Source, Argonne National Laboratory, 9700 South Cass Avenue, Argonne, IL 60439, USA

R. MACHARRIE
AT&T Bell Laboratories, Murray Hill, NJ 07974, USA

A new technique has been used for the early stages of crystallization of amorphous materials, like metallic alloys. *In situ* X-ray diffraction has been performed during the early stages of crystallization of $Fe_{80}B_{20}$. The samples are resistively heated to 600° C in a customized vacuum chamber. A programmable charge-coupled device detector records simultaneously the evolution of the three phases: α-Fe, Fe_3B and Fe_2B in the minute scale. This is the first in situ X-ray diffraction study of this system in these temperature and time scales. Interesting behaviours have been seen: appearance and disappearance of phases, α-Fe supersaturation solution in boron (found for the first time in this compound), and migration of B out of the α-Fe matrix. The two-dimensional diffraction pictures show topography irregularities indicating crystallite inhomogeneties.

1. Introduction

Metallic glasses, regardless of the way they are prepared, are not in configurational equilibrium but are relaxing slowly by a homogeneous process towards an "ideal" metastable amorphous state of lower energy. This system possesses the inherent possibility of transforming into a more stable crystalline state. However, the most promising properties of metallic glasses, e.g. the excellent magnetic behaviour or the high hardness and strength combined with ductility and high corrosion resistance, have been found to deteriorate drastically during crystallization. Understanding the micromechanisms of crystallization in order to impede or control the process is, therefore, a prerequisite for most applications.

The crystallization of the Fe–B system has been studied by several methods: differential scanning calorimetry (DSC) [1], Mössbauer spectroscopy [2], scanning electron (SEM) and transmission electron (TEM) microscopy [3], and X-ray diffraction [4]. The previous X-ray studies conducted on Fe–B have generally been realized on a long time-scale (one hour or more for X-ray diffraction, one day or more for Mössbauer spectroscopy), and at high temperatures. The previous X-ray diffraction studies are summarized in Table I [5–9]. Moreover, most of the X-ray diffraction so far has been taken at room temperature; the experiments are not done *in situ*.

The purpose of this experiment is to elucidate nucleation and growth characteristics evolution of the crystalline phases in an $Fe_{80}B_{20}$ metallic glass. Hence, early stages of crystallization of $Fe_{80}B_{20}$ have been studied with *in situ* X-ray diffraction at the National Synchrotron Light Source (NSLS). A programmable charge-coupled device (CCD) detector records the evolution of diffraction peaks versus temperature in the minute range. This two-dimensional area detector allows one to record full diffraction patterns within a large field of view. Hence, the appearance and growth of the α-Fe, Fe_3B and Fe_2B phases, and the disappearance of the Fe_3B phase, have been recorded in the field of view of the CCD chip without any mechanical motion of the CCD detector during the experiment. Moreover, the detector's high dynamic range enables one to look at strong and weak peaks at the same time. Interesting characteristics have been put in evidence, like phase dynamics, α-Fe supersaturated solution in B, and crystallite growth. Studies of the irregularities in the two-dimensional recorded diffraction peaks lead to topography. Crystallite inhomogeneities have been put in evidence. This first *in situ* X-ray diffraction-

TABLE I X-ray diffraction for crystallization studies of $Fe_{80}B_{20}$ amorphous alloys

Reference	Heat treatment[a]
[5]	$T = 780\,^{\circ}C$, $\Delta t = 1$ s–8 h
[6]	$T = 300$–$900\,^{\circ}C$, $\Delta T/\Delta t = 100\,^{\circ}C\ h^{-1}$, $\Delta t = 1$ h
[7]	$T = 400$–$1000\,^{\circ}C$, $\Delta T/\Delta t = 15\,^{\circ}C\ h^{-1}$
[8]	$T = 300$–$900\,^{\circ}C$, $\Delta t = 1$–2 h
[9]	$T = 300$–$600\,^{\circ}C$, $\Delta t = 1$ h

[a] T is the temperature range at which data were recorded. $\Delta T/\Delta t$ was the heating rate. Δt is the period during which a sample was heated at a constant temperature.

0022–2461 © *1993 US Government*

topography of the beginning of $Fe_{80}B_{20}$ crystallization in the minute range uses a promising new technique to study crystallization of amorphous materials.

2. Experimental procedure

2.1. Beamline characteristics

The X6 beamline at NSLS presents a double-crystal flat Si(2 2 0) monochromator that allows one to tune the photon energy. The beam energy was set at 7 keV, which is below the Fe fluorescence edge. A rocking curve of Si(1 0 0) using the (4 0 0) reflection gives an energy spread of 1×10^{-3} (Fig. 1). The flux is 5×10^{9} ph s^{-1} mm^{-2} for an electron beam intensity of 200 mA.

The influence of the horizontal length x of the beam is usually not taken into account for vertical geometry diffraction, because of the regular use of one-dimensional detectors. The beam of horizontal length x can be considered as made of infinitely thin beams. For one of these infinitely thin beams, it is easy to understand the geometry of the diffraction pattern if we visualize the collection of crystal orientations by holding the Ewald sphere fixed and allowing each and every r^*_{hkl} to take on all possible orientations (Fig. 2). The notation r^*_{hkl} describes the reciprocal vector corresponding to the Miller indices. The different infinitesimal beams define adjacent Ewald spheres. The two extreme spheres are distant from the beam length. The intersection of these extreme spheres with the r^*_{hkl} sphere is two cones distant from the beam horizontal length x (3.5 mm for this experiment). The maximum difference of position between the two extreme circles on the CCD chip plane is 60 μm (3 pixels). This distance is much smaller than the intrinsic variation of the peak position, typically 20 pixels (corresponding to 2.6×10^{-3} rad), due to inhomogeneities (crystallites size). Thus, the contribution of the horizontal length of the beam can be neglected.

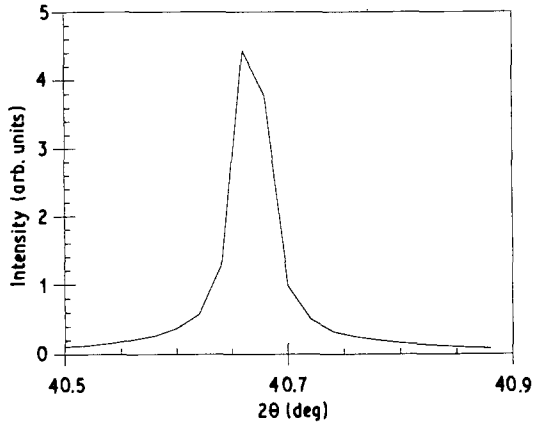

Figure 1 Rocking curve of Si(1 0 0) using the (4 0 0) reflection. It gives an energy spread of 1×10^{-3}.

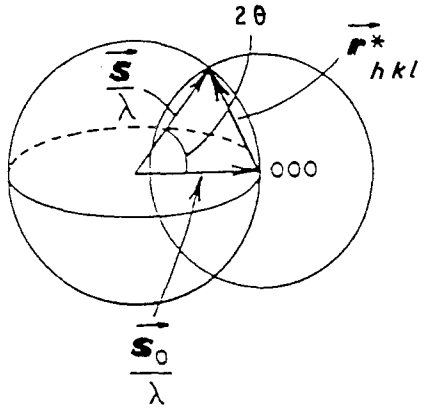

Figure 2 Intersection of the Ewald sphere with r^*_{hkl} sphere generated by random powder generations.

2.2 Samples

The $Fe_{80}B_{20}$ samples are from Allied Chemical Co. of Morristown, New Jersey under the trade name MG 2605. They are realized with the melt-spinning method [10]. The studied samples were aged over a few years. In order to prevent the oxidation of Fe during the heat-treatment, the samples are placed in a small vacuum chamber mounted at the centre of the six-circle Huber diffractometer. A typical pressure in this aluminium chamber with a Kapton window is 10^{-3} torr. The sample is clamped on two small copper rods to which a current of few amperes is applied (Fig. 3). The rods are also linked with an isolated spring to prevent the sample from bowing or breaking during the heating or cooling phases. It should be noted that none of the samples broke, although they are very brittle once crystallized. The rest of the mount is in Macor (a machinable ceramic).

Geometrical considerations indicate that the ribbon sample should be placed at a high ϕ angle, so that the beam footprint on the sample would be smaller and the diffracted peak thinner. For the experiment, the ϕ angle is equal to 39° and the height of the beam is 1.4 mm. This contributes to a geometrical diffracted peak width of 0.488 mm.

2.3. CCD detector

A fully programmable CCD detector records the diffraction peaks. The CAMAC-based system is extremely flexible [11]. Time-resolved experiments like rapid thermal annealing have already been performed [12]. The *in situ* crystallization was performed in the

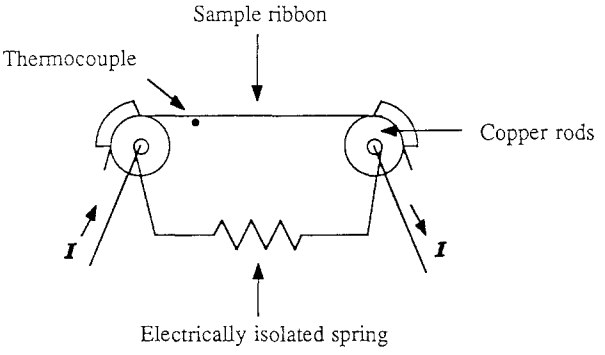

Figure 3 Sample holder having two copper rods to which a few amperes of current are applied. The rods are linked with an isolated spring to prevent the sample from bowing or breaking during the heating or cooling phases.

vertical geometry, and the detector was attached to the 2θ arm of the diffractometer. The diffraction patterns of a polycrystalline sample are cones of semi-apex angle 2θ [13]. The main α-Fe reflection is located at a 2θ angle of 51.83°. At the location of the CCD chip (17 cm from the sample), the diffracted pattern corresponds to a large circle of radius 216 mm. The 13 mm long chip intercepts 0.06 rad (3.5°). The maximum distance between the intercepted arc and its chord is 60 μm on the CCD chip plane (3 pixels). This distance is much smaller than the intrinsic variation of the peak position, typically 20 pixels (corresponding to 2.6×10^{-3} rad), due to inhomogeneities (crystallites size). So, the diffracted peaks can be assumed to be parallel to the columns of the CCD chip. Hence, the rows can be summed in order to improve the statistics. If the phenomenon to be studied is faster than a few seconds, the rows would be summed in the serial register of the chip itself. On the other hand, if the time constant of the phenomenon is larger than a few seconds, frames would be recorded typically every few seconds, and rows can be added later in the software. As the kinetics of the crystallization of $Fe_{80}B_{20}$ are quite slow, the second method was used.

2.4. Experimental set-up

The experimental set-up is represented in Fig. 4. The CCD chip allows one to record the evolution of different peaks at the same time within a field of view of 2.9° in the geometry that is used. The sample must be very carefully aligned with respect to the beam in order to observe the three different growing diffracted peaks corresponding to the three phases that appear within the detector field of view during the crystallization. The sample is successively heated at different temperatures, from room temperature to 600 °C.

3. Results

The observed diffracted peaks are summarized in Table II. The earliest crystallization is detected in the sample heated from room temperature to 380 °C in 11 min. This is the first time that the $Fe_{80}B_{20}$ crystallization has been detected at such an early stage at low temperature. Frames are recorded for different isothermal states (Fig. 5). The amount of crystallized Fe_3B does not change at 400 °C, but decreases at 500 °C and disappears at 600 °C (metastable phase). At 300 °C, the main peak is much more intense than the (321) Fe_3B peak. Both phases, α-Fe and Fe_3B, appear in the same range of temperature around 300 °C (eutectic crystallization). Then, the part of the crystallized hypo-eutectoid alloy (α-Fe) keeps increasing from 300 to 600 °C. The main peak becomes more intense, sharper, and moves towards the smaller 2θ angle as the crystallization occurs (Table III). Between 300 and 400 °C the main peak shifts 15 pixels (i.e. 2×10^{-3} rad), but the position of the small peak (Fe_3B) does not change at all. The displacement of the main peak does not come from a displacement of the sample or from a thermal dilatation but represents an

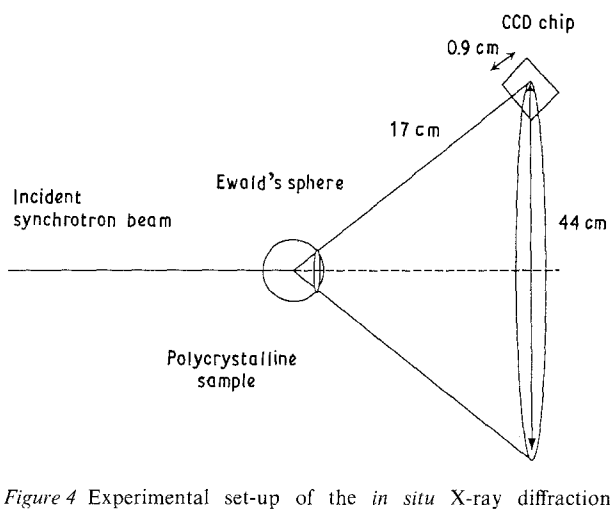

Figure 4 Experimental set-up of the *in situ* X-ray diffraction $Fe_{80}B_{20}$.

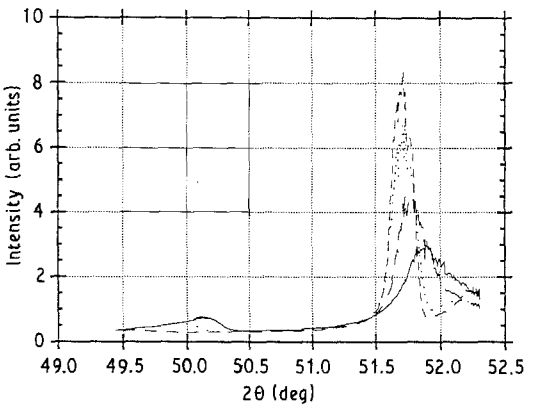

Figure 5 X-ray diffraction peaks obtained by summing the CCD chip rows. From low to high angle: Fe_3B, α-Fe, Fe_2B. (—) 300 °C, (– –) 400 °C, (···) 500 °C, (– – –) 600 °C.

TABLE II Diffracted peaks observed at an energy of 7 keV (classified with increasing 2θ)[a]

Compound	(*hkl*)	I/I_1	*d* (nm)	2θ (deg)
Fe_3B	321	100	0.2088	50.20
	330, 112	100	0.2028	51.79
α-Fe	110	100	0.20268	51.83
Fe_2B	211	100	0.20129	52.21

[a] The data are taken from the Joint Committee on Powder Diffraction Standards (JCPDS), 1983. The column I/I_1 provides the relative intensities for one compound. The strongest line in the pattern has a ratio of 100. The parameter *d* (nm) is the interplanar spacing. Note that the Fe_3B (330, 112) and α-Fe (110) reflections coincide.

TABLE III α-Fe *d* spacing increase, $\Delta d/d$[a]

T (°C)	$\Delta d/d$ (10^{-3})
400	4.1
500	6.5
600	6.8

[a] The reference *d* spacing is the one at 300 °C; $\Delta d/d = \cot\theta \times \Delta\theta$.

intrinsic physical behaviour related to the increase of the d spacing.

For temperature higher than 500 °C, the main peak presents a shoulder at an angle 0.4° higher than the peak maximum position. This additional peak is clearly visible for a more advanced crystallization and corresponds to the primitive tetragonal Fe_2B (211) peak. The appearance of this Fe_2B phase is clearly linked with the disappearance of the Fe_3B phase. The integrated intensity does not change much with the temperature. However, the maximum intensity increases significantly with temperature. From 300 to 600 °C, the α-Fe crystallized fraction does not increase much (Table IV), but the grain size increases through conglomeration. α-Fe coalesces and precipitates out of the matrix. This is in good agreement with previous work [5]. The numerous small nuclei get transformed into fewer large nuclei.

4. Discussion

4.1. Nuclei growth predominance

The devitrification is driven by the nucleation and growth processes. In section 3, it has been mentioned that the α-Fe crystallized fraction does not increase much, but the grain size increases through conglomeration. In $Fe_{80}B_{20}$, the quenched-in nuclei are numerous (about 10^{18} m^{-3}) [14]. The nuclei formed during the quenching period are retained in the glass at room temperature. As the temperature gets high, the nuclei grow. The growth of quenched-in nuclei is expected to be the dominant mechanism at low annealing temperatures. However, at high annealing temperatures, the predominant behaviour is transient and steady-state nucleation.

4.2. Crystallite inhomogeneities

The apparent size L (volumetric average) of crystalline grains can be calculated from the diffraction peak width at half maximum [15]:

$$L = \frac{0.9\lambda}{\cos\theta_0 \Delta'(2\theta)},$$

where λ is the wavelength, θ_0 is the Bragg angle and $\Delta'(2\theta)$ is the full width at half maximum (FWHM).

The peaks shown in Fig. 3 correspond to diffraction peaks integrated over a large part of the sample, similar in a way to the diffracted peaks obtained during powder crystal rotation. For numerical applications, $\Delta'(2\theta)$ is the FWHM of the diffracted peak deconvoluted with the geometrical beam effects. The grain size increases with temperature (Table V). The numerical values are in good agreement with previous work done with an electron microscope [16]. At high temperature (600 °C), intense spots can be seen in the main peak (Fig. 6). This behaviour comes from the existence of larger crystallites. Typically, for a 5-pixel wide spot, the diameter of the grain is 270 nm. The spot size behaves as a local probe of the sample.

The use of the kinematic theory is justified. This theory is used in the case of an "ideally imperfect" crystal. This crystal is formed of an aggregate of small blocks, less than a few micrometres in size. The blocks can thus be rotated slightly, one with respect to the other, or displaced by a distance that is not exactly a lattice vector, so that the waves diffracted by two neighbouring blocks are incoherent. On the other hand, the dynamical theory is used for "perfect" crystals. This theory is useful for crystals where the average crystallite size is a few times the extinction depth in the crystal. The studied sample corresponds to the ideally imperfect crystal; hence, the kinematical theory is used in this paper.

4.3. α-Fe(B) supersaturated solution

The dilatation contribution for the d spacing of Fe (Table VI) has been calculated using the coefficient of linear thermal expansion for Fe. This dilatation effect is negligible in the observed d spacing increase. The d spacing variation comes from the existence of a supersaturated solution of α-Fe(B). This behaviour has already been found in some Fe–B systems [6]. It is emphasized that this finding of the existence of a single phase of α-Fe(B) just after the crystallization is important, because no report on this point has been found in the literature for $Fe_{80}B_{20}$. This B migration out of the α-Fe matrix has not been observed by Mössbauer spectroscopy which is very sensitive to lattice changes (hyperfine interactions), because statistics must be accumulated for, typically, one or two days.

TABLE IV Crystallization variations for α-Fe and Fe_3B (reference taken at 300 °C)

T (°C)	α-Fe	Fe_3B
300	1	1
400	0.97	1.03
500	1.06	0.45
600	1.24	0.00

TABLE V Average α-Fe crystallite diameter calculated from the FWHM of the peak resulting from a row sum (i.e. integrated over a large region of the sample

T (°C)	L (nm)
300	18
400	38
500	68
600	100

TABLE VI Coefficient of linear thermal expansion α for Fe [13] (reference temperature: 20 °C) and dilatation contribution for the d spacing of Fe (reference temperature: 300 °C)

T (°C)	α (10^6) ($°C^{-1}$)	$\Delta d/d$ (10^{-3})
400	1.443	0.109
500	1.458	0.218
600	1.471	0.327

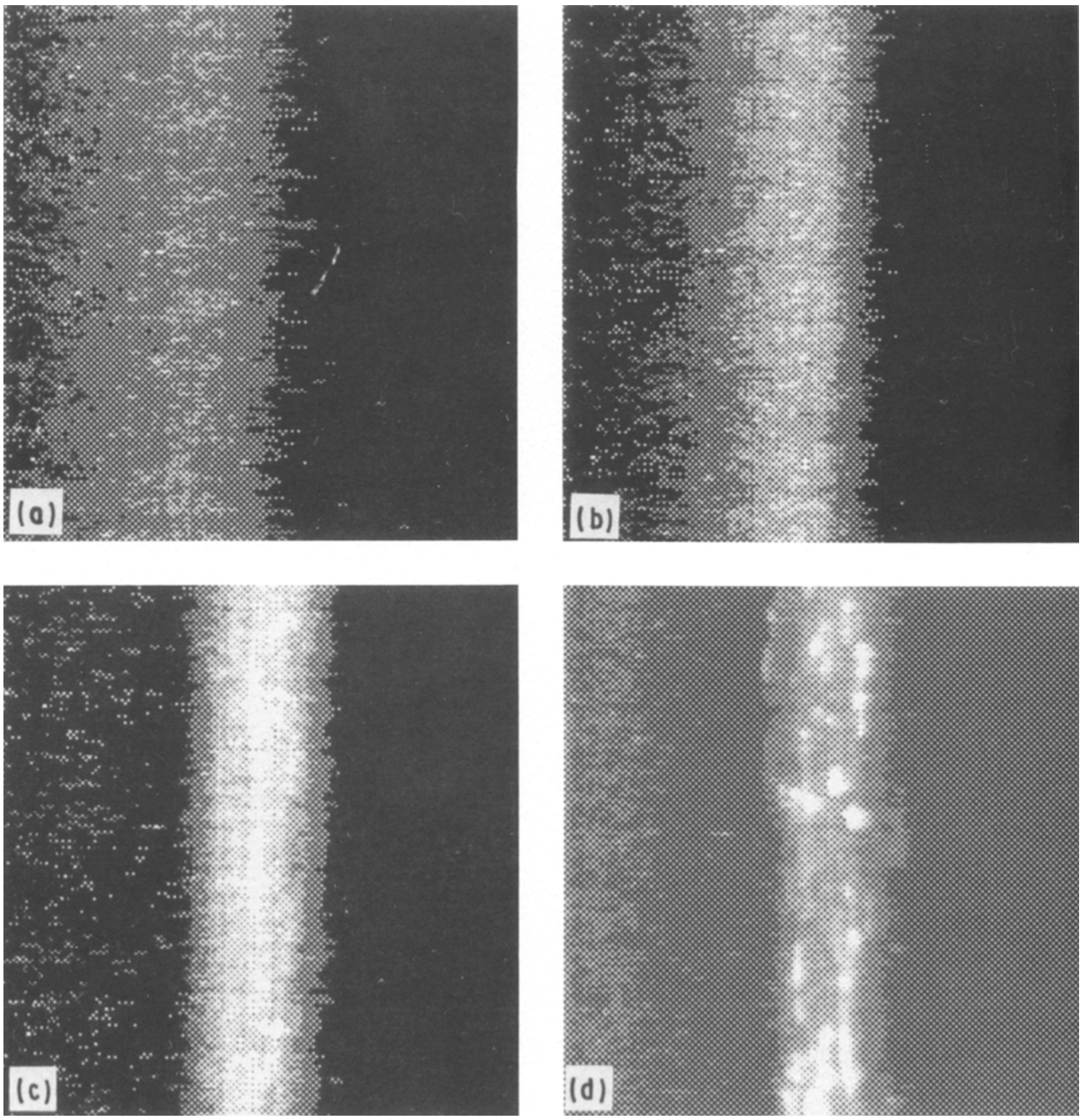

Figure 6 Full X-ray diffraction pictures obtained with the CCD detector at different temperatures: (a) 300 °C, (b) 400 °C, (c) 500 °C, (d) 600 °C. The peaks become more intense and sharper as the temperature increases. At 600 °C, very intense spots reveal the presence of large crystallite sizes.

4.4. Different phases

The phase diagram of Fe–B alloy [6] indicates that, after 360 °C, the Fe_3B phase begins to appear in the amorphous compound. For a temperature higher than 380 °C, the phases α-Fe and Fe_3B are present and after 690 °C, the phases α-Fe and Fe_2B coexist. The results are in good agreement with the phase diagram, except that the appearance of these events has been detected earlier (at lower temperatures) in our work. Around 500 °C, B still migrates from the α-Fe matrix to the Fe_3B matrix and then to the Fe_2B matrix. Further crystallization of α-Fe occurs. At this stage, the decomposition of Fe_3B takes place. Finally, the Fe_3B phase disappears around 600 °C, after transformation into α-Fe and Fe_2B. Crystallization of α-Fe is still occurring.

The respective proportion of the different phases can be estimated (Table VII). The integrated intensities of the peaks are proportional to the square of the charge number Z of the elements and to the quantities of the elements that are present. In the experimental temperature range, the predominant phase is α-Fe.

TABLE VII Proportion of the different phases (in number of atoms) at different temperatures

T (°C)	n_{Fe}	n_{Fe_3B}	n_{Fe_2B}
300	0.81	0.19	0
400	0.81	0.19	0
500	0.56	0.05	0.38
600	0.65	0	0.35

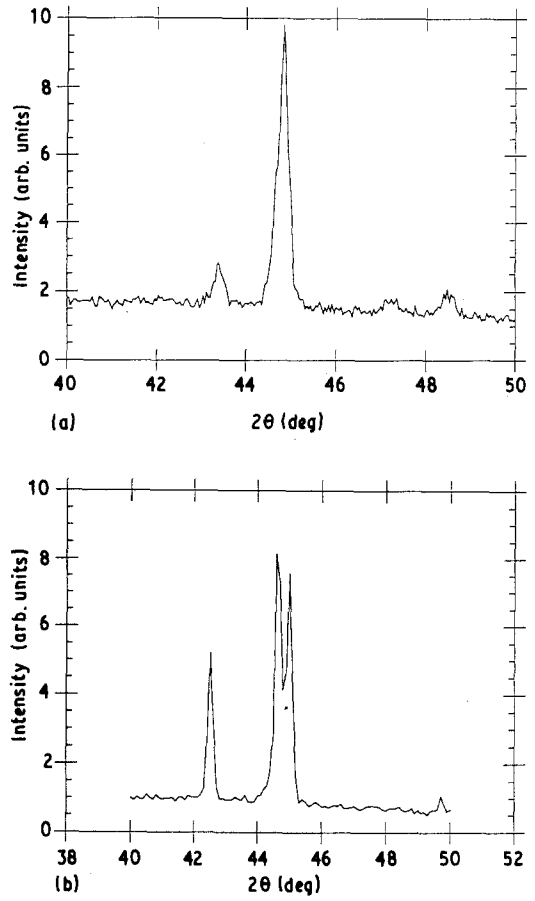

Figure 7 θ–2θ scans of $Fe_{80}B_{20}$ at (a) 600°C and (b) 900°C.

For low temperatures (less than 500°C), Fe_3B is approximately four times less preponderant. For higher temperatures, Fe_2B is half as preponderant as the α-Fe phase.

4.5. Comparison with a static $Fe_{80}B_{20}$ crystallization study

The same batch samples were annealed in a small furnace at 600°C for 1 h. θ–2θ scan was then performed at room temperature (Fig. 7a). The only existing components at this stage are α-Fe and Fe_3B. Although the final temperature is the same, the products obtained for the *in situ* experiment versus this static one are different. The decomposition of Fe_3B into α-Fe and Fe_2B has not yet taken place. The heat-treatment sequences are determinant for the reactions in the $Fe_{80}B_{20}$ system. A heat treatment of 1.5 or 2 h at 600°C leads to the same conclusion. A θ–2θ scan of a sample annealed at 900°C for 1 h shows that the components at this stage are α-Fe and Fe_2B (Fig. 7b).

5. Conclusion

An *in situ* X-ray diffraction of $Fe_{80}B_{20}$ samples resistively heated to 600°C has been performed with a programmable CCD detector at NSLS. The earliest crystallization has been found to occur in samples heated from room temperature to 380°C in 11 min. Phase dynamics, crystallite inhomogeneities and α-Fe supersaturated solution in B have been studied. A very interesting experiment would be to perform similar *in situ* X-ray diffraction in order to study the crystallization of $Fe_{75}B_{25}$. At temperatures less than 900°C, this system decomposes only into Fe_3B, so the kinetics should be faster [6]. One of the difficulties in detecting the early stages of crystallization of the metallic glasses is because of the weakness of the diffracted peaks. The use of the CCD area detector allows one to improve the statistics by a factor equal to the number of rows or columns, typically 500 to 1000. The new generation of synchrotrons will be of utmost importance for carrying out such experiments. This new diffraction/topography method, based on a programmable CCD detector, is promising for the study of the early stages of crystallization of amorphous materials.

Acknowledgements

The authors wish to thank Gopal Shenoy and Dennis Mills for their great support; also Joe Arko and Ron Hopf for their invaluable help assisting us. It is a pleasure to thank Pedro Montano, and Marc Engbretson for the use of X6B at NSLS. This work is supported by US Department of Energy, BES-Materials Science, under grant contract No. W-31-109-ENG-38.

References

1. E. E. ALP, K. M. SIMON, M. SAPOROSCHENKO and W. E. BROWER Jr, *J. Non-Cryst. Solids* **61-62** (1984) 871.
2. E. E. ALP, Thesis, Southern Illinois University (1984).
3. A. L. GREER, *J. Non-Cryst. Solids* **61–62** (1984) 737.
4. J. M. DUBOIS and G. LECAER, *Phys. Status Solidi(a)* **64** (1981) 275.
5. O. T. INAL, L. KELLER and F. G. YOST, *J. Mater. Sci.* **15** (1980) 1947.
6. M. TAKAHASHI, M. KOSHIMURA and T. ABUZUKA, *Jpn. J. Appl. Phys.* **20** (1981) 1821.
7. Y. KHAN and M. SOSTARICH, *Z. Metallkde* **72** (1981) 256.
8. J. A. CUSIDO, A. ISALGUE and J. TEJADA, *Phys. Status Solidi(a)* **87** (1985) 169.
9. P. TLOMAK, S. J. PIERZ, L. J. PAULSON and W. E. BROWER Jr. *Mater. Sci Engng* **97** (1988) 369.
10. H. A. DAVIES, in "Amorphous Metallic Alloys, " edited by F. E. Luborsky (Butterworths).
11. C. BRIZARD and B. RODRICKS, in Proceedings of SRI Conference, Chester, UK, 1991, *Rev. Sci. Instrum.* in press.
12. R. CLARKE, W. PASSOS, W. LOWE, B. RODRICKS and C. BRIZARD, *Phys. Rev. Lett.* **60** (1991) 317.
13. L. H. SCHWARTZ and J. B. COHEN, "Diffraction from Materials", 2nd Edn (MRE).
14. A. L. GREER, *Mater. Sci Engng* **97** (1988) 285.
15. A. GUINIER, "X-ray Diffraction" (Freeman).
16. P. TLOMAK, S. J. PIERZ, L. J. PAULSON and W. E. BROWER Jr, *Mater. Sci. Engng* **97** (1988) 369.

Received 2 September 1991
and accepted 24 July 1992